Imaging Agents

DOI: 10.1002/ange.201106686

A High-Performance Ytterbium-Based Nanoparticulate Contrast Agent for In Vivo X-Ray Computed Tomography Imaging**

*Yanlan Liu, Kelong Ai, Jianhua Liu, Qinghai Yuan, Yangyang He, and Lehui Lu**

X-ray computed tomography (CT) is one of the most widely used imaging procedures in diagnostic medicine due to its many advantages that include cost effectiveness, deep tissue penetration, and high resolution.[1–5] Currently, small iodinated molecules are routinely used for in vivo contrast enhancement in the clinical setting. Iodinated molecules can effectively absorb X-rays but suffer from short circulation lifetime and potential renal toxicity.[6] Another notable disadvantage is the relatively low K-edge of iodine (33 keV). X-rays that are optimized for this K-edge have a higher potential for damaging tissues. Nanoparticulate CT contrast agents that comprise high atomic number (high-*Z*) metal elements (mainly focused on gold, platinum, bismuth, and tantalum) have been proved to be a powerful tool to address these issues.[7–13] These nanoparticulate CT contrast agents have exhibited good imaging effects, acceptable safety profiles, and long circulation half times in vivo. Nevertheless, these metal elements, in principle, would not display prominent superiority in contrast efficacy with respect to clinical iodinated agents under normal operating conditions (120 kVp), because their attenuation characteristics are mismatched with the X-ray photon energy used in clinical CT.[14a] Moreover, administration of a large amount of contrast agent is often required in CT imaging, and the very low abundance of these elements in the earth's crust is most likely to result in huge cost issues.[14b]

Compared to the currently available Au-, Pt-, Bi-, and Ta-based nanomaterials, Yb-based nanostructures hold great promise as CT contrast agents. The benefits of Yb in nanomaterials are as follows: 1) its K-edge energy (61 keV) is located just within the higher-energy region of the X-ray spectrum used in clinical CT, hence ensuring both higher intrinsic contrast and lower radiation exposure to the patients;[15a,b] 2) low toxicity when encapsulated in the stable nanoparticle;[15c] 3) the highest abundance in the earth's crust among these metals,[14b] and thus it has a potential for industrial production; and 4) Yb is a well-known component of upconversion luminescence nanocrystals, which provides a particularly useful platform for the design of multimodal imaging nanoprobes without additional modification of functionalities. Nevertheless, to our knowledge, Yb-based nanoparticulate CT contrast agents have remained unexplored until now.

Herein, we describe the first example of Yb-based nanoparticulate CT contrast agents. For these nanoparticles, not only the surface modification but also the control over the size and morphology can be easily achieved. More significantly, owing to the attenuation characteristics of Yb-based nanoparticles, which are matched with the X-ray photon energy used in clinical applications, they can offer a much higher contrast efficacy compared to clinical iodinated agents at 120 kVp. Together with long circulation time and low toxicity, these nanoparticles can act as a high-performance CT contrast agent for in vivo angiography and bimodal image-guided lymph node mapping. Moreover, the near-infrared to visible or near-infrared to near-infrared (NIR-to-Vis or NIR-to-NIR) upconversion luminescence of the Yb-nanoparticles can effectively avoid the tissue damage and poor tissue penetration associated with UV excitation. Finally, doping gadolinium into these nanoparticles further endows them with magnetic resonance imaging (MRI) capability.

$NaYbF_4$:Er nanoparticles stabilized with oleic acid (OA-UCNPs) were synthesized by the strategy schematically illustrated in Figure 1a. These nanoparticles could be well-dispersed in many organic solvents without any detectable agglomeration. The transmission electron microscopy (TEM) image showed that undoped $NaYbF_4$:Er nanoparticles were highly monodisperse but had irregular shapes and different sizes (Figure 1b). The control over size and shape of these nanoparticles could be easily achieved through doping Gd^{3+} ions into these nanoparticles during the synthetic process. Uniformly sized nanoparticles with regular shapes were produced at a Gd^{3+} concentration of 20 mol% or higher (Figure 1d,e). This control over size and shape of nanoparticles is of great importance in their biological and clinical applications, because the circulation time in vivo and interactions of the nanoparticles with various cells are highly dependent on their size, shape, and surface properties.[16,17] Furthermore, high-resolution TEM images revealed lattice fringes with a spacing of about 0.31 nm for both the undoped $NaYbF_4$:Er and the 10 mol% Gd-doped samples, corresponding to the lattice spacing in the (111) planes of cubic-phase $NaYbF_4$. For the samples with higher Gd concentrations, the

[*] Y. L. Liu, K. L. Ai, Prof. L. H. Lu
State Key Laboratory of Electroanalytical Chemistry, Changchun Institute of Applied Chemistry, Chinese Academy of Sciences
5625 Renmin Street, Changchun 130022 (P.R. China)
E-mail: lehuilu@ciac.jl.cn
J. H. Liu, Prof. Q. H. Yuan
Department of Radiology, the Second Hospital of Jilin University
Norman Bethune, Changchun, 130022 (P.R. China)
Y. Y. He
Department of Pathology, the Second Hospital of Jilin University
Norman Bethune, Changchun, 130022 (P.R. China)

[**] Financial support by NSFC (Nos. 21125521, 21075117), the National Basic Research Program of China (973 Program, No. 2010CB933600), and the "Hundred Talents Project" of the Chinese Academy of Science is gratefully acknowledged.

Supporting information for this article is available on the WWW under http://dx.doi.org/10.1002/anie.201106686.

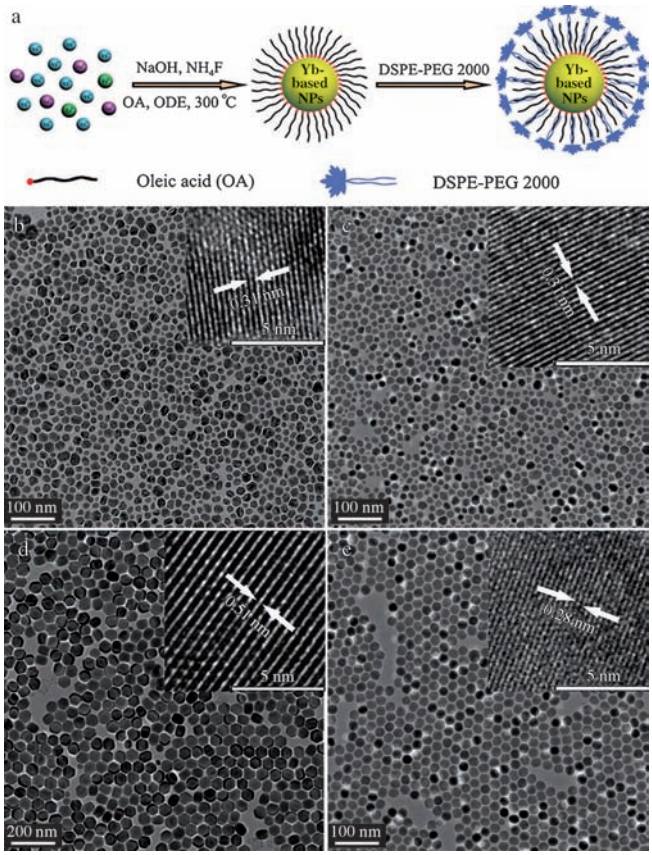

Figure 1. a) Schematic illustration of the synthesis and surface modification of OA-stabilized upconverting nanoparticles (UCNPs). Blue Yb^{3+}, pink Gd^{3+}, and green Er^{3+}. TEM and high-resolution TEM images of $NaYbF_4$:Er nanoparticles doped with various concentrations of Gd in chloroform: b) without doping, c) 10 mol%, d) 20 mol% (diameter ca. 52 nm), and e) 30 mol% (diameter ca. 20 nm). The insets show the corresponding high-resolution TEM images and arrows highlight *d* spacing.

observed *d* spacing values of 0.51 and 0.28 nm for 20 and 30 mol% Gd-doped samples were highly consistent with (100) and (101) phases of the hexagonal $NaYbF_4$ crystalline structures, respectively. This cubic-to-hexagonal phase conversion of these samples as the Gd concentration increased was evident in the X-ray diffraction (XRD) patterns as well (Figure 2a). It has been demonstrated that cubic sodium rare-earth fluoride ($NaREF_4$) has one type of high-symmetry cation site, while hexagonal-phase $NaREF_4$ consists of an ordered array of F^- ions with two types of low-symmetry cation sites selectively occupied by Na^+ and RE^{3+} ions, leading to significant electron-cloud distortion. The Gd dopant, with larger ionic radii than Yb, exhibits a high tendency towards electron-cloud distortion owing to increased dipole polarizability and thereby favors the hexagonal structures.[18] The Gd doping was confirmed by energy-dispersive X-ray analysis (EDAX) and X-ray photoelectron spectroscopy (XPS) (Figures S1 and S2 in the Supporting Information).[19] The exact molar concentrations of Gd in the final products, determined by inductively coupled plasma mass spectrometry (ICP-MS), were very similar to the stoichiometric ratios (Table S1 in the Supporting Information).

Because the insolubility of the as-prepared OA-UCNPs in water impeded their further applications in vivo, we modified the surface of the OA-UCNPs with DSPE-PEG 2000 to yield PEG-UCNPs. DSPE-PEG 2000, a well-known biocompatible polymer, is often used for drug delivery and has been used to stabilize a variety of other nanoparticles for in vivo imaging.[20–23] The example of 20 mol% Gd-doped OA-UCNPs (Figure 2b) shows that the as-prepared PEG-UCNPs were well-dispersed in water without any detectable agglomeration, and they remained stable for days. Even after dialysis for one week in blood serum and physiological saline, no leaching of free Yb^{3+} or Gd^{3+} ions was detected by ICP-MS. The successful modification of PEG was confirmed by FTIR spectroscopy (Figure 2c). Two new bands at 1737 and 1109 cm^{-1} in the FTIR spectrum of PEG-UCNPs were assigned to the stretching vibration of the carboxyl ester and the ether bond of PEG chains, respectively.[24] The amount of PEG on the surface of nanoparticles, as assessed by thermogravimetric analysis, was approximately 20% (Figure S3 in the Supporting Information). The favorable dispersion of PEG-UCNPs in aqueous media indicated their high potential for applications in vivo.

To assess CT contrast efficacy, we next compared the X-ray absorption of PEG-UCNPs to that of iobitridol (a most widely used CT contrast agent in clinical applications) in solution. Both agents exhibited signal enhancement as the concentration of the agent increased (Figure 3a,b). A good linear correlation between the Hounsfield units (HU) value and the concentration of Yb (or I) was observed. Nevertheless, at equivalent concentrations, the X-ray absorption of PEG-UCNPs was much higher than that of iobitridol (Figure 3a). Considering that the high-*Z* metal elements contribute to the dominant X-ray attenuation of the nanoparticulate CT contrast agents we also compared, as an identification experiment, the X-ray attenuation of several metallic salts to assess the contrast efficacy of PEG-UCNPs compared to currently available Au-, Pt-, Bi-, and Ta-based nanoparticulate CT contrast agents (Figure S4c in the Supporting Information). The result illustrated that Yb gave the highest HU value at 120 kVp, the generally used voltage in clinical applications. This finding is perhaps not surprising, because the K-edge of Yb (61 keV) is located just within the higher-energy region of the X-ray spectrum at this voltage. In contrast, the K-edge values of Au, Pt, Bi, and Ta were found to be deviated from this region (see Figure S4 in the Supporting Information for the details). These results revealed that the as-prepared PEG-UCNPs were greatly superior to Au-, Pt-, Bi-, and Ta-based nanoparticulatein vivo CT contrast agents at 120 KVp.

Prior to using PEG-UCNPs for in vivo imaging, we first tested their cytotoxicity using the methyl thiazolyl tetrazolium (MTT) assay. This crucial factor must be established in determining the suitability of this agent for specific applications in experimental small-animal and ultimately in clinical studies. Encouragingly, cell viability was not hindered by PEG-UCNPs up to a concentration of 3.2 mg Yb ml^{-1}, thereby revealing the remarkably low cytotoxicity of PEG-

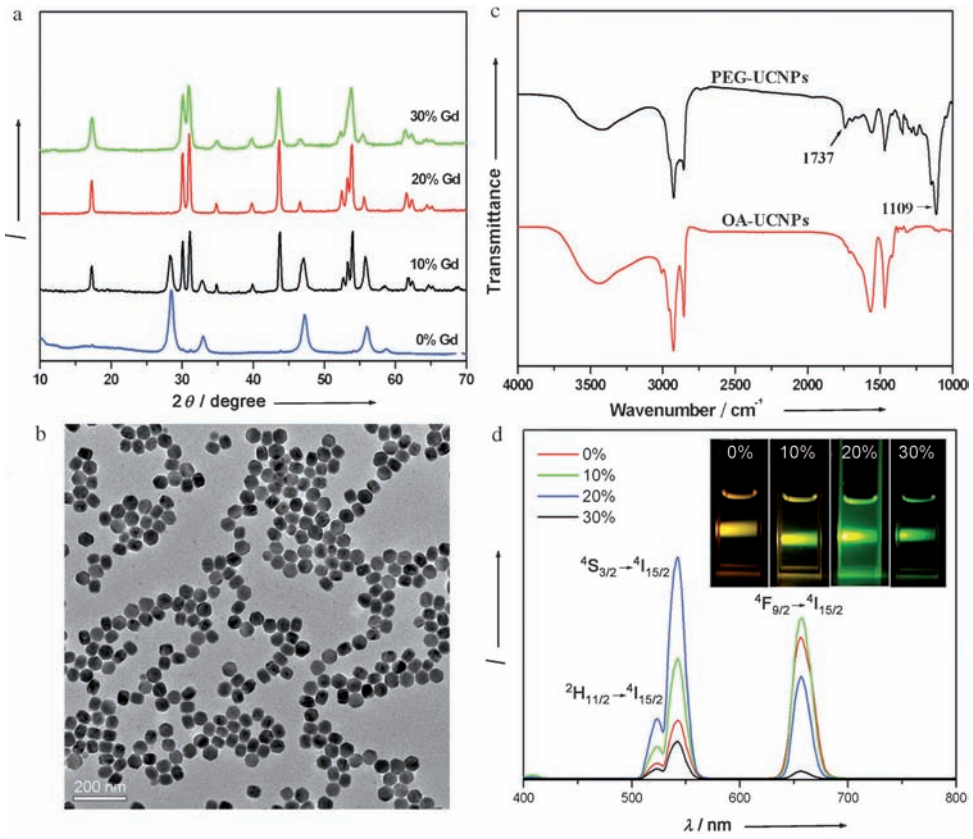

Figure 2. a) XRD patterns of Gd-doped $NaYbF_4$:Er nanoparticles with varied concentrations of Gd (JCPDS nos. 77-2043 and 27-1427 for cubic and hexagonal $NaYbF_4$ crystalline structure, respectively). b) TEM image of PEG-UCNPs dispersed in water. c) FTIR spectra of OA-UCNPs and PEG-UCNPs. d) Room-temperature IR-to-Vis upconversion luminescence spectra of Gd-doped $NaYbF_4$:Er nanoparticles with different concentrations of Gd. The electronic states of Er are given next to the corresponding peaks. The inset shows the upconversion luminescence photograph of the Gd-doped $NaYbF_4$:Er nanoparticles with different concentrations of Gd under excitation at 980 nm.

UCNPs (Figure 3c). We also investigated the behavior of PEG-UCNPs in living cells. CT and fluorescence images confirmed the PEG-UCNPs were internalized by HeLa cells, and the internalization was concentration-dependent (Figure 3d). Conversely, hardly any uptake by cells was observed for iobitridol even at a concentration of 10 mg I ml^{-1}, which was three times higher than that of Yb in PEG-UCNPs. The internalization of PEG-UCNPs by cells is important in clinical applications, particularly for tumor target imaging and detection in vivo.

These encouraging results prompted us to evaluate the feasibility of PEG-UCNPs as in vivo CT imaging probes. A solution of PEG-UCNPs was intravenously administered to a rat and the distribution of the particles was tracked by X-ray CT imaging at timed intervals (Figure 4). A clear enhancement of the signal of the heart could be observed at least within 20 min without an appreciable loss of contrast, and a more careful look at the 3D-renderings of CT images showed evident enhancement of the signals of great vessels within this same period of time as well. Long-lasting circulation in vessels is a key factor in many biomedical applications, including vascular imaging and diagnosis of diseases. After one hour, the enhancement of the signal for the heart and vascular tissue decreased rapidly (Figure 4a, Table S2 in the Supporting Information). Nevertheless, the gradual enhancement of the signals for liver and spleen continued for over two hours. This long-lasting liver-signal enhancement may improve the detection of the hepatic metastases.[25] Furthermore, intravenous administration of PEG-UCNPs at a concentration of half of the above dosage in another rat resulted in the clear enhancement of the signals of these organs similar to the above results (Figure S5 and Table S3 in the Supporting Information). This reduced dose requirement is highly beneficial in a contrast agent, because it reduces potential adverse effects in patients in clinical applications.

For comparison, we imaged a different rat after intravenous administration of iobitridol using the same CT protocol (Figure S6 and Table S4 in the Supporting Information). Delayed imaging three minutes after injection confirmed that most of the iobitridol had accumulated in the urinary organs (kidney and bladder), and no contrast was detected in the heart, vessels, or other organs that contained macrophages, thereby indicating the short circulation time and rapid vascular permeation of iobitridol. These inherent limitations of iobitridol also made it unsuitable for lymph node delivery to improve cancer staging, which would be helpful for avoiding unnecessary surgery.[13,26] In contrast, the long circulation of PEG-UCNPs in vessels, as illustrated above, would enable the nanoparticles to migrate to the lymph nodes through lymphatic drainage. Figure S7 in the Supporting Information shows the CT image of a rat after subcutaneous administration of PEG-UCNPs solution into the paw; regional lymph nodes were clearly contrasted. This result demonstrates that PEG-UCNPs should be able to precisely detect cancer metastasis by lymph node mapping.

To further determine whether PEG-UCNPs caused any harmful effect or disease, we investigated their long-term toxicity by assessing histological changes in several susceptible organs, including heart, liver, and spleen (Figure 5). The rat was dissected three weeks after a single PEG-UCNPs injection, and the organs were stained with hematoxylin and eosin (H&E). We observed no tissue damage or any other adverse effect associated with the administration of PEG-

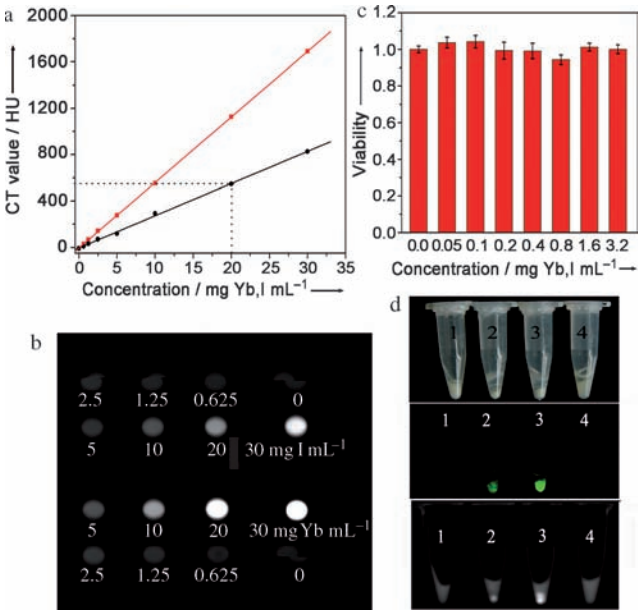

Figure 3. a) CT value (HU) of PEG-UCNPs (red squares) and iobitridol (black circles) as a function of the concentration of Yb (red trace) and I (black trace), respectively. b) CT images of solutions of PEG-UCNPs and iobitridol with different concentrations of Yb and I, respectively. c) Cell viability of A549 cells after incubation with increased concentration of PEG-UCNPs for 24 h. d) Cell uptake analysis: bright field images (top), upconversion luminescence images (middle), and CT images (bottom) of washed pellets from HeLa cells incubated without contrast agent (1), with different concentrations of PEG-UCNPs (1.6 and 3.2 mg Yb mL^{-1} for (2) and (3), respectively), and iobitridol (10 mg I mL^{-1} for (4)) for 24 h.

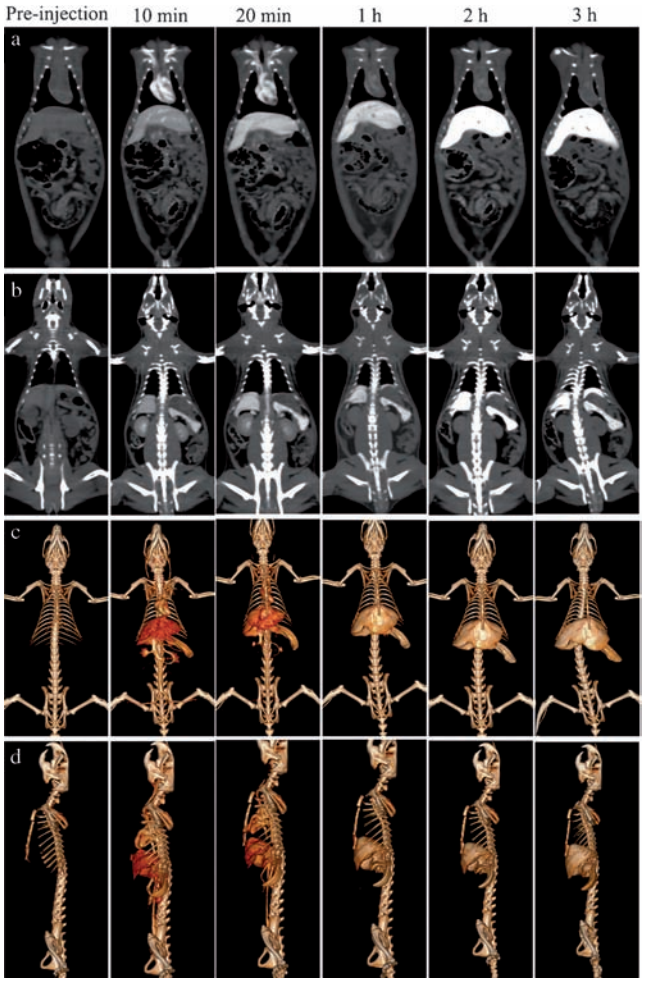

Figure 4. In vivo CT coronal view images of a rat after intravenous injection of 1 mL PEG-UCNPs (70 mg Yb mL^{-1}) solution at timed intervals. a) Heart and liver. b) Spleen and kidney. c, d) The corresponding 3D renderings of in vivo CT images.

UCNPs. This result suggested that PEG-UCNPs hold great promise as an injectable CT contrast agent for applications in biological medicine. Furthermore, ICP-MS analysis detected an elimination of about 34% of PEG-UCNPs from the rat body during this period of time. The relatively slow elimination has also been observed in other nanoparticulate imaging agents.[11a]

$NaYbF_4$ is well-known as a host material for NIR-Vis upconversion luminescence (UCL). These UCNPs have great advantages in biological imaging, because the use of NIR for excitation allows a greater penetration depth in biological tissues and results in lower phototoxicity and reduced background.[27–29] Interestingly, in the presence of the Gd dopant (20 mol%), the UCL intensity of the UCNPs was significantly enhanced under excitation at 980 nm (Figure 2d). We attributed this enhancement to the cubic-to-hexagonal phase conversion and the size increase of nanocrystals.[30,31] After modification with PEG, we noticed no obvious change in the UCL wavelength except a slight decrease in UCL intensity arising from the change of ligand and solvent (Figure S8 in the Supporting Information). Figure S9 in the Supporting Information demonstrated the potential value of PEG-UCNPs as luminescent probes for in vivo imaging. An aliquot (100 μL) of PEG-UCNPs dispersed in water was subcutaneously injected into a Kunming mouse. From Figure S9b in the Supporting Information, a bright emission was clearly visible at the injection site. Moreover, this bright emission was also

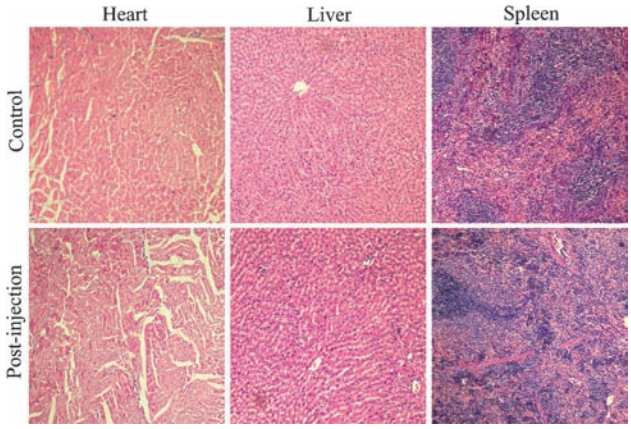

Figure 5. Histological changes in the heart, liver, and spleen of the rat three weeks after intravenous injection of a single dose of PEG-UCNPs solution. These organs are stained with H&E and observed under a light microscope at 100× magnification.The control shows the organ images of the rat without injection of PEG-UCNPs solution.

detected from HeLa cells treated with PEG-UCNPs, thereby revealing that the application of PEG-UCNPs could be extended to tumor-targeting fluorescence imaging (Figure 3d middle panel, and Figure S10 in the Supporting Information). Notably, the emission could be tuned to the NIR region (800 nm), further avoiding the poor tissue penetration and large amounts of scattering of light of visible wavelength, thus enhancing the detection sensitivity (Figure S11 in the Supporting Information).[32]

The Gd in PEG-UCNPs can accelerate longitudinal (T_1) relaxation of water protons and can exert bright contrast in regions where the nanoprobes localize,[33] and we therefore evaluated the capability of PEG-UCNPs as MRI contrast agents. Figure S12b in the Supporting Information demonstrated the T_1-weighted MR image of the PEG-UCNPs with different Gd concentrations. The MR signal was enhanced linearly as the Gd concentration increased over the range from 0 to 8 mM. The specific relaxivity values (r_1) calculated from the slope of the concentration-dependent relaxation rate was 0.41 $mM^{-1}s^{-1}$, comparable to the values of previous Gd-based and MnO T_1 contrast agents.[22,34] Significantly, no toxic free Gd^{3+} ion leached from the PEG-UCNPs even after one week (Figure S12c in the Supporting Information), thus indicating that PEG-UCNPs were stable and capable of use for in vivo imaging without encountering Gd^{3+} poisoning. To assess their feasibility as in vivo MRI contrast agents, 1 mL of PEG-UCNPs dispersion with a Gd concentration of 10 mM was intravenously administered to a rat and the animal was imaged by a 1.5 T human clinical scanner. T_1-weighted enhancement was clearly visible (Figure S13 in the Supporting Information).

In summary, we have, for the first time, developed an Yb-based nanoparticulate CT contrast agent. Its feasibility as an in vivo CT contrast agent was intensively investigated, and the results revealed that PEG-UCNPs showed low cytotoxicity and long circulation time in vivo. More significantly, they provided a much higher efficacy compared to a clinical iodinate agent in present use, and they could be even more effective than currently available Au-, Pt-, Bi-, and Ta-based nanoparticulate CT contrast agents under normal operating conditions (120 kVp). This improvement is primarily attributed to the K-edge energy of Yb that locates within the higher energy region of the X-ray spectrum. Furthermore, Gd-doping in these nanoparticles endowed them with enhanced fluorescence and NMR imaging capabilities. This multimodal imaging property would allow these nanoparticles to provide a better reliability of the collected data and have great potential in biological and medical applications. Nevertheless, the relatively slow elimination of PEG-UCNPs from the rat body associated with their large size is an issue of concern. The preparation of nanoparticles with size reduced below 10 nm and in vivo animal experiments are underway.

Experimental Section

Materials: The rare-earth oxides Yb_2O_3, Er_2O_3, and Tm_2O_3 (purity > 99.99%) were obtained from the Changchun Hepalink rare-earth materials company. Oleic acid and octadecene were purchased from Sigma-Aldrich. Iobitridol was purchased from Guerbet (France). 1,2-distearoyl-*sn*-glycero-3-phosphoethanolamine-*N*-{methoxy-[poly(ethylene glycol)]-2000} (DSPE-PEG2000) was purchased from shanghai advanced viecle technology l.t.d. co (China). Other chemicals were analytical grade and used as received without further purification.

Synthesis of OA-stabilized UCNPs: Yb_2O_3, Er_2O_3, and Gd_2O_3 were separately dissolved in excess 1:1 hydrochloric acid aqueous solution at 80°C. After the hydrochloric acid and water evaporated at 140°C, the resulting powders were redispersed in water to yield the $YbCl_3$ (1M), $ErCl_3$ (0.1M), and $GdCl_3$ (1M) aqueous stock solutions. In a typical procedure for the synthesis of $NaYbF_4$:2%Er nanoparticles, $YbCl_3$ aqueous solution (1.47 mL, 1M) and $ErCl_3$ aqueous solution (0.3 mL, 0.1M) were injected in a 50 mL flask. After removal of the water, oleic acid (15 mL) and octadecene (ODE, 23 mL) were added. The solution was heated to 160°C under Ar protection to yield a homogeneous solution, which was subsequently cooled to room temperature. Subsequently, methanol solution (15 mL) containing NH_4F (0.222 g, 6 mmol) and NaOH (0.15 g, 3.75 mmol) was added slowly. After vigorous stirring for 30 min, the solution was slowly heated to 220°C to remove the residual water and impurities with low boiling point under Ar protection. Thereafter, the temperature was increased to 300°C at a rate of 10°C min^{-1} and remained at this temperature for 1.5 h. After cooling to room temperature in ambient conditions, the nanoparticles were obtained through centrifugation at 10000 rpm for 20 min and washed two times with ethanol. Finally, the nanoparticles were redispersed in chloroform. The Gd-doped $NaYbF_4$:Er nanoparticles were synthesized according to the same procedure by replacing part of $YbCl_3$ with $GdCl_3$ aqueous stock solutions under the stoichiometric molar ratios.

Surface modification of OA-stabilized UCNPs: Water-soluble UCNPs were prepared according to the reported method.[22] UCNPs in chloroform (10 mL, 10 mg mL^{-1}) were added into a solution of DSPE-PEG2000 in chloroform (20 mL, 5 mg mL^{-1}) and stirred for ten minutes. The solvent was evaporated and the mixture was maintained at 60°C for one hour under vacuum. Water (10 mL) was injected. After filtration using a 0.2 μm cellulose acetate syringe filter and centrifugation, the excess PEG was removed.

Received: September 20, 2011
Published online: December 30, 2011

Keywords: imaging agents · magnetic resonance imaging · nanoparticles · X-ray computed tomography · ytterbium

[1] W. A. Kalender, *Phys. Med. Biol.* **2006**, *51*, R29 – R43.
[2] K. E. deKrafft, Z. Xie, G. Cao, S. Tran, L. Ma, O. Z. Zhou, W. Lin, *Angew. Chem.* **2009**, *121*, 10085 – 10088; *Angew. Chem. Int. Ed.* **2009**, *48*, 9901 – 9904.
[3] N. F. Schwenzer, F. Springer, C. Schraml, N. Stefan, J. Machann, F. Schick, *J. Hepatol.* **2009**, *51*, 433 – 445.
[4] A. de Vries, E. Custers, J. Lub, S. Bosch, K. Nicolay, H. Grüll, *Biomaterials* **2010**, *31*, 6537 – 6544.
[5] F. Hyafil et al., *Nat. Med.* **2007**, *13*, 636 – 641.
[6] a) C. Haller, I. Hizoh, *Invest. Radiol.* **2004**, *39*, 149 – 154; b) I. Hizoh, C. Haller, *Invest. Radiol.* **2002**, *37*, 428 – 434.
[7] W. Eck, A. I. Nicholson, H. Zentgraf, W. Semmler, S. Bartling, *Nano Lett.* **2010**, *10*, 2318 – 2322.
[8] C. j. Xu, G. A. Tung, S. H. Sun, *Chem. Mater.* **2008**, *20*, 4167 – 4169.
[9] D. Kim, Y. Y. Jeong, S. Jon, *ACS Nano* **2010**, *4*, 3689 – 3696.
[10] V. Kattumuri et al., *Small* **2007**, *3*, 333 – 341.
[11] a) O. Rabin, J. M. Perez, J. Grimm, G. Wojtkiewicz, R. Weissleder, *Nat. Mater.* **2006**, *5*, 118 – 122; b) D. Pan, T. A. Williams, A. Senpan, J. S. Allen, M. J. Scott, P. J. Gaffney, S. A. Wickline, G. M. Lanza, *J. Am. Chem. Soc.* **2009**, *131*, 15522 – 15527; c) K. L.

Ai, Y. L. Liu, J. H. Liu, Q. H. Yuan, Y. Y. He, L. H. Lu, *Adv. Mater.* **2011**, *23*, 4886 – 4891.
[12] S. W. Chou, Y. H. Shau, P. C. Wu, Y. S. Yang, D. B. Shieh, C. C. Chen, *J. Am. Chem. Soc.* **2010**, *132*, 13270 – 13278.
[13] M. H. Oh et al., *J. Am. Chem. Soc.* **2011**, *133*, 5508 – 5515.
[14] a) S. B. Yu, A. D. Watson, *Chem. Rev.* **1999**, *99*, 2353 – 2377; b) J. Emsley, *The Elements*, Oxford University Press, New York, **1989**.
[15] a) W. Krause, G. Schuhmann-Giampieri, M. Bauer, W. R. Press, P. Muschick, *Invest. Radiol.* **1996**, *31*, 502 – 511; b) S. A. Schmitz, S. Wagner, G. Schuhmann-Giampieri, W. Krause, M. Bollow, K. J. Wolf, *Radiology* **1997**, *205*, 361 – 366; c) L. Q. Xiong, T. S. Yang, Y. Yang, C. J. Xu, F. Y. Li, *Biomaterials* **2010**, *31*, 7078 – 7085.
[16] X. L. Huang, X. Teng, D. Chen, F. Q. Tang, J. Q. He, *Biomaterials* **2010**, *31*, 438 – 448.
[17] B. D. Chithrani, A. A. Ghazani, W. C. Chan, *Nano Lett.* **2006**, *6*, 662 – 668.
[18] F. Wang et al., *Nature* **2010**, *463*, 1061 – 1065.
[19] H. S. Yang, S. Santra, G. A. Walter, P. H. Holloway, *Adv. Mater.* **2006**, *18*, 2890 – 2894.
[20] B. Dubertret, P. Skourides, D. J. Norris, V. Noireaux, A. H. Brivanlou, A. Libchaber, *Science* **2002**, *298*, 1759 – 1762.
[21] Y. D. Jin, C. X. Jia, S. W. Huang, M. O'Donnell, X. H. Gao, *Nat. Commun.* **2010**, DOI: 10.1038/ncomms1042.
[22] H. B. Na et al., *Angew. Chem.* **2007**, *119, 5493 – 5497; Angew. Chem. Int. Ed.* **2007**, 46, 5397 – 5401; *Angew. Chem. Int. Ed.* **2007**, *46*, 5397 – 5401.
[23] Y. I. Park et al., *Adv. Mater.* **2009**, *21*, 4467 – 4471.
[24] D. Liu, W. Wu, J. Ling, S. Wen, N. Gu, X. Zhang, *Adv. Funct. Mater.* **2011**, *21*, 1498 – 1504.
[25] D. Kim, S. Park, J. H. Lee, Y. Y. Jeong, S. Jon, *J. Am. Chem. Soc.* **2007**, *129*, 7661 – 7665.
[26] M. G. Harisinghani, J. Barentsz, P. F. Hahn, W. M. Deserno, S. Tabatabaei, C. Hulsbergen van de Kaa, J. Rosette, R. Weissleder, *N. Engl. J. Med.* **2003**, *348*, 2491 – 2499.
[27] Q. Zhan, J. Qian, H. Liang, G. Somesfalean, D. Wang, S. He, Z. Zhang, S. Andersson-Engels, *ACS Nano* **2011**, *5*, 3744 – 3757.
[28] O. Ehlert, R. Thomann, M. Darbandi, T. Nann, *ACS Nano* **2008**, *2*, 120 – 124.
[29] Z. Q. Li, Y. Zhang, S. Jiang, *Adv. Mater.* **2008**, *20*, 4765 – 4769.
[30] G. Chen, T. Y. Ohulchanskyy, R. Kumar, H. Ågren, P. N. Prasad, *ACS Nano* **2010**, *4*, 3163 – 3168.
[31] H. X. Mai, Y. W. Zhang, R. Si, Z. G. Yan, L. d. Sun, L. P. You, C. H. Yan, *J. Am. Chem. Soc.* **2006**, *128*, 6426 – 6436.
[32] J. M. Baumes, J. J. Gassensmith, J. Giblin, J. J. Lee, A. G. White, W. J. Culligan, W. M. Leevy, M. Kuno, B. D. Smith, *Nat. Chem.* **2010**, *2*, 1025 – 1030.
[33] Y. L. Liu, K. L. Ai, Q. H. Yuan, L. H. Lu, *Biomaterials* **2011**, *32*, 1185 – 1192.
[34] a) R. Kumar, M. Nyk, T. Y. Ohulchanskyy, C. A. Flask, P. N. Prasad, *Adv. Funct. Mater.* **2009**, *19*, 853 – 859; b) J. Zhou, M. X. Yu, Y. Sun, X. Z. Zhang, X. J. Zhu, Z. H. Wu, D. M. Wu, F. Y. Li, *Biomaterials* **2011**, *32*, 1148 – 1156.

